Hindawi
Advances in Materials Science and Engineering
Volume 2022, Article ID 9431143, 7 pages
https://doi.org/10.1155/2022/9431143

Research Article

Rock Fracture Response Exposed to Hydraulic Fracturing: Insight into the Effect of Injection Rate on Aperture Pattern

Bo Zhang,[1,2,3] **Xinyi Cui**,[1,2,3] **Linjun Wang**,[1,2,3] **and Xiaodi Fu**[1,2,3]

[1]*Architectural Engineering College, Guizhou Minzu University, Guiyang 550025, China*
[2]*Guizhou Provincial Engineering Geological Disaster Prevention and Control Engineering Research Center of Guizhou Minzu University, Guiyang 550025, China*
[3]*The Karst Environmental Geological Hazard Prevention Laboratory of Guizhou Minzu University, Guiyang 550025, China*

Correspondence should be addressed to Bo Zhang; zhangbo_dzs@126.com

Received 10 November 2021; Revised 20 February 2022; Accepted 24 February 2022; Published 20 March 2022

Academic Editor: Zhengyang Song

Injection rate is critical to hydraulic fracturing operation, especially to the hydraulic fracture aperture, which affects the proppant and methane migration. In this study, hydraulic fracturing experiments were carried out on shale specimens to investigate the influence of injection rate on hydraulic fracture aperture. According to the experimental results, when the injection rate increases, the average aperture of hydraulic fracture shows a significant linear increase. For different injection rate, the average aperture of stimulated natural fracture is always slightly greater than that of newly opened fracture. Compared with a low injection rate, the fracture apertures induced by the largest injection rate are evenly distributed in more intervals and approximately conform to the normal distribution. The research results can provide a theoretical basis for enhancing the fracture conductivity of hydraulic fracturing in shale reservoirs.

1. Introduction

Hydraulic fracturing technology is critical in the unconventional energy field, especially for shale gas [1–3]. The hydraulic fracturing operation could stimulate the natural fractures and open the new fractures in the shale reservoir. The initiation, propagation, and coalescence of these fractures make up the network where the methane flow [4–8].

Injection rate is one of the most important factors for the success of hydraulic fracturing operation [9–11]. De Pater et al. [12] conducted experiments and numerical simulations in early time, to investigate the influence of injection rate on fracture patterns. Using true triaxial test and high-energy CT scanning system, Guo et al. [13] and Zou et al. [14] showed that injection rates with intervals had different effects on fracture complexity in hydraulic fracturing for shale, and variable injection rate fracturing could increase the complexity of the fracture network. Wang et al. [15] indicated that the impact of injection rate on hydraulic fracturing treatment depends on the characteristics of the shale reservoir. Seong et al. [16] investigated the evolution of the breakdown pressure and the fracture initiation pressure, which indicated that high injection rate results in an increased value of the two kinds of pressures. For brittle rocks, the induced fractures are very sensitive to loading conditions [17, 18].

The abovementioned research studies about injection rate in hydraulic fracturing focused on fracture complexity, rather than fracture aperture. The aperture of hydraulic fractures is essential for proppant and methane migration. However, the study published on it is very limited [19, 20]. In this work, hydraulic fracturing experiments of shale with different injection rates were conducted by a true triaxial test system. Then, a portable industrial electron microscope was utilized to measure the open aperture of fractures induced by hydraulic fracturing. Finally, the apertures of different types of fractures are calculated through mathematical statistics, and the relationship between the aperture and injection rate was established.

2. Experiment Equipment and Scheme

2.1. Experiment Equipment. In order to simulate the three-dimensional stress state of shale reservoirs, the hydraulic fracturing experiments are conducted in an electro-hydraulic servo true triaxial test system (Figure 1). The triaxial pressure cell of this system could contain a cubic specimen with a side length of 30 cm, and each pair of pistons was pressurized independently with an oil pressure pump. The hydraulic fracturing pump pressure servo control system has a maximum displacement of 1 L/min and a maximum output pressure of 80 MPa.

Figure 1: True triaxial hydraulic fracturing test system.

2.2. Specimen Preparation. The shale blocks are taken from the outcrop of the Longmaxi Formation in China, where the natural fractures are very developed. In the Fenggang block of the Longmaxi formation, the high-angle fractures account for 56.4% of natural fractures, and the rest are low-angle fractures and parallel-bedded fractures [21]. These shale rocks were processed into standard specimen of 30 cm × 30 cm × 30 cm with a disk saw. A drill bit with an outer diameter of 12 mm was used to prefabricate a 15 cm deep borehole perpendicular to the bedding plane of shale specimens, to model the perforations in a horizontal well. A high-strength steel pipe with an outer diameter of 10 mm, an inner diameter of 6 mm, and a length of 13 cm is installed in the borehole to facilitate the injection of fracturing fluid into the specimen. High-strength epoxy resin glue is used to bond the steel pipe to the shale sample, and the final specimen is shown in Figures 2 and 3. It should be noted that the bottom of the steel pipe is wrapped with tissue paper and plastic wrap, to prevent epoxy resin from flowing into the borehole, causing a blockage at the end of the steel pipe. The physical and mechanical parameters of shale are shown in Table 1.

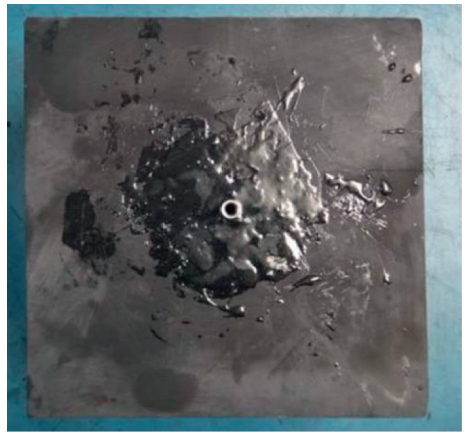

Figure 2: The shale specimen after processing.

2.3. Experiment Scheme. The confining pressure conditions for this experiment are $\sigma_v = 12$ MPa, $\sigma_H = 14$ MPa, and $\sigma_h = 10$ MPa. In this study, the direction of σ_v is perpendicular to the bedding (Figure 3), and the specific test parameters are shown in Table 2. The ordinary water is taken as fracturing fluids, which is injected into shale specimens at the constant injection rate.

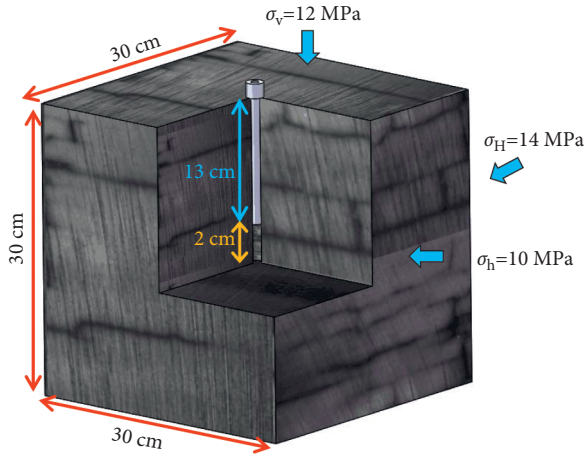

Figure 3: Three-dimensional (3D) graph of shale specimen.

The specific test steps are as follows:

(1) Dip a clean towel with clean water, and wipe clean on the six surfaces of the shale specimen. Take pictures of the surfaces with a digital camera, and use drawing software to record the distribution of natural fractures before the test.

(2) Put the prepared shale specimen into the true triaxial stress loading chamber and complete the triaxial stress loading. At the same time, the hydraulic loading system of pumping is started, and the computer collects various test data in time.

(3) When the total volume of fracturing fluid is injected into 900 ml, the hydraulic fracturing experiment ends. The hydraulic loading system is stopped, and the stress in the true triaxial loading chamber is unloaded to zero.

(4) Disassemble the sample, use a digital camera to photograph each surface of the specimen after fracturing, and use drawing software for post-processing of hydraulic fractures.

(5) Take a portable industrial electron microscope to measure the opening aperture of hydraulic fractures, including stimulated natural fractures and newly opened fractures.

Table 1: Physical and mechanical parameters of shale.

Cohesion stress (MPa)	Friction angle (MPa)	Tension stress (MPa)	Elastic modulus (GPa)	Poisson ratio
31.6	26.8	7.6	32.3	0.23

Table 2: Test conditions for hydraulic fracturing.

Specimen number	σ_v (MPa)	σ_H (MPa)	σ_h (MPa)	Injection rate (ml/min)
S1	12	14	10	40
S2	12	14	10	100
S3	12	14	10	150

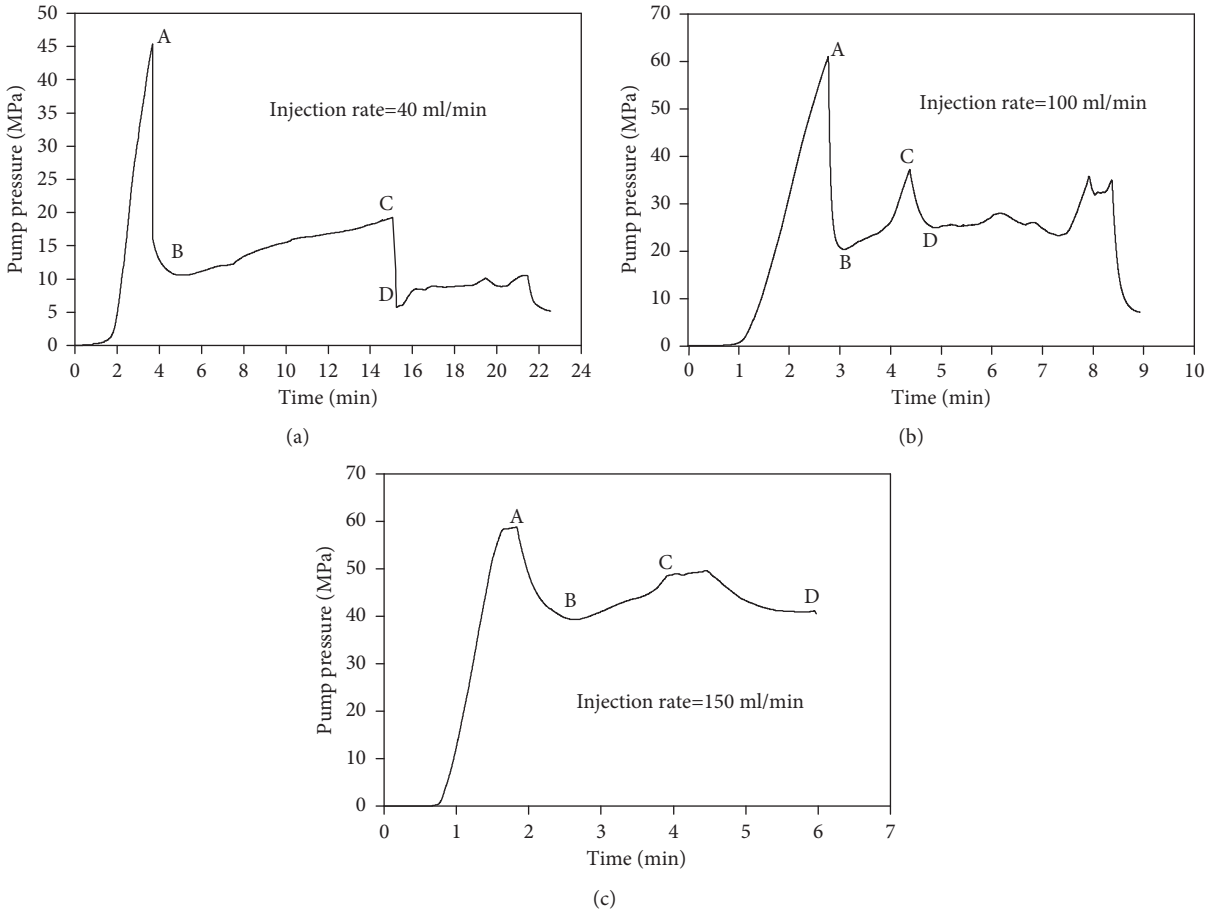

Figure 4: Pumping pressure-time curve for hydraulic fracturing experiments: (a) S1; (b) S2; (c) S3.

3. Experiment Results and Analysis

3.1. Pump Pressure-Time Curve. Specimen S1 was injected with fracturing fluid with a constant injection rate of 40 ml/min, and the breakdown pressure was 45.4 MPa. As shown in Figure 4(a), the pump pressure curve of S1 is rapidly to point A, then the specimen broke and the pump pressure decreased (point B). After the natural fractures were stimulated, the pump pressure dropped (point D), and the pump pressure fluctuated only slightly.

S2 was injected with fracturing fluid with a constant injection rate of 100 ml/min, and the breakdown pressure was 61 MPa. The pump pressure-time curve is shown in Figure 4(b). The reason for the curve pattern may be as follows. When the breakdown pressure is reached (point A), the primary hydraulic fracture of the shale sample is initiated, which makes the fluid flow into the hydraulic fracture rapidly, resulting in the decrease of pump pressure (point B). Then, due to the existence of highly cemented and closed natural fractures in the sample, the propagation of hydraulic fractures was blocked, and the pump pressure was raised again (point C). When the natural fractures were stimulated, the fluid further leaked into these fractures, causing the pump pressure to drop (point D).

S3 was injected with fracturing fluid with a constant injection rate of 150 ml/min, and the breakdown pressure

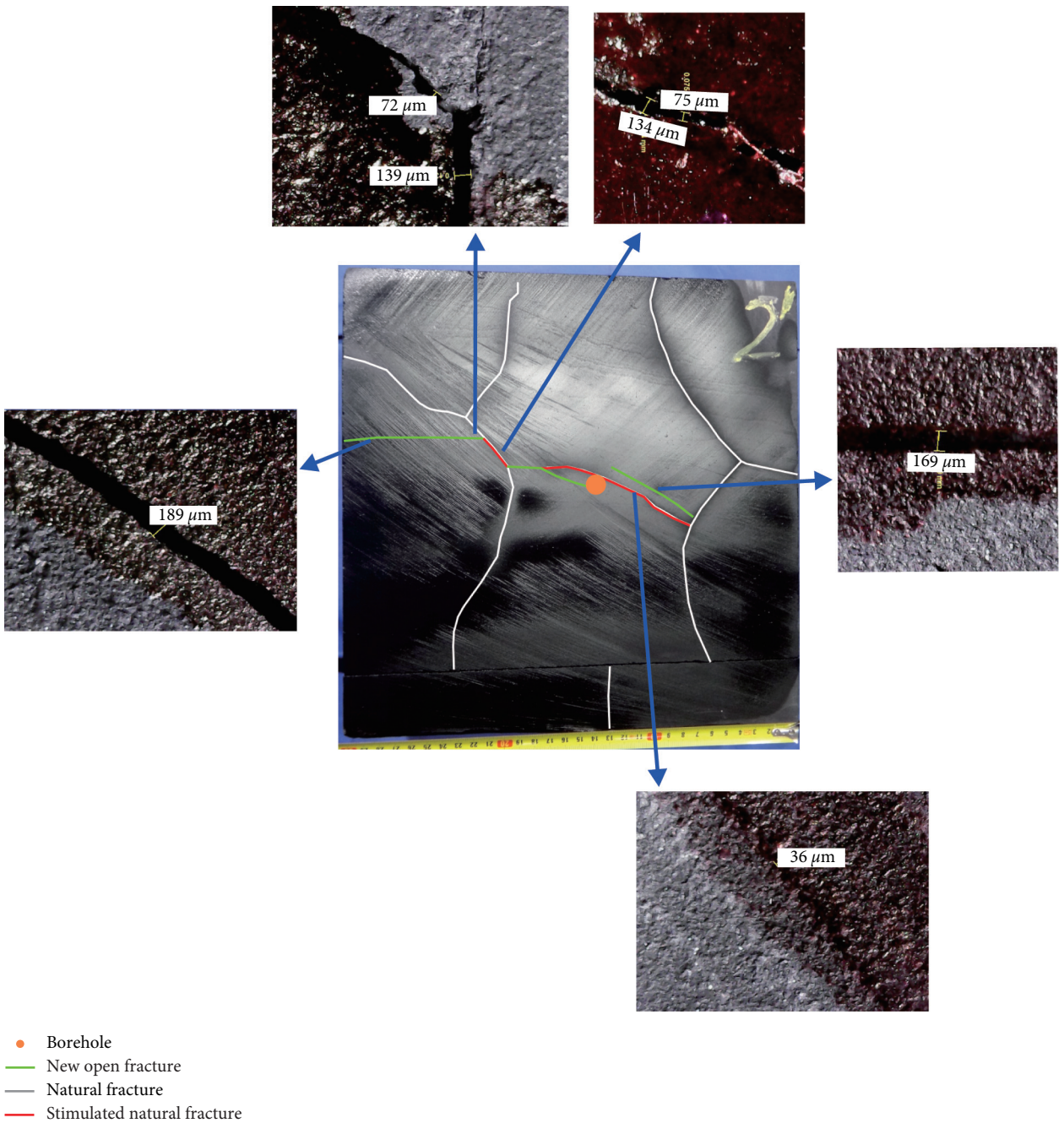

Figure 5: Various types of fracture of the shale specimens after hydraulic fracturing.

was 58.8 MPa. As shown in Figure 4(c), the pump pressure curve of S3 was significantly different from that of S1 and S2. The fluctuation times of S3 are less than that of S1, and the pump pressure of S3 could still be maintained at a higher pressure (about 40 MPa) after the pump pressure dropped.

3.2. Analysis of Fracture Aperture of Specimens. Electron microscope was utilized in order to scan and measure the fracture apertures of the shale specimens after hydraulic fracturing. Taking the fractures in surface 2′ of S3 as an example, the types of fractures are shown in Figure 5. The green, red, and white lines represent, respectively, newly opened fracture (NOF), stimulated natural fracture (SNF), and natural fracture (NF).

After statistics of the fracture apertures of each specimen, the average aperture of 159 fractures which contain 43 NOFs and 116 SNFs, was calculated and listed in Table 3 according to the type of fracture. In this study, the hydraulic fracture (HF) contains both of NOF and SNF.

It can be seen from Table 3 that the average value of the fracture aperture of all types of fractures increases with the injection rate. When the injection rate increases from 40 ml/min to 150 ml/min, the HF apertures corresponding to S1 to

Table 3: Aperture of fractures on the surfaces of specimens.

Fracture type	The average aperture of S1 (μm)	The average aperture of S2 (μm)	The average aperture of S3 (μm)
NOF	54.67	110.32	152.33
SNF	68.94	119.37	165.29
HF	65.48	115.88	163.35
Ratio of SNF/NOF	1.26	1.08	1.09

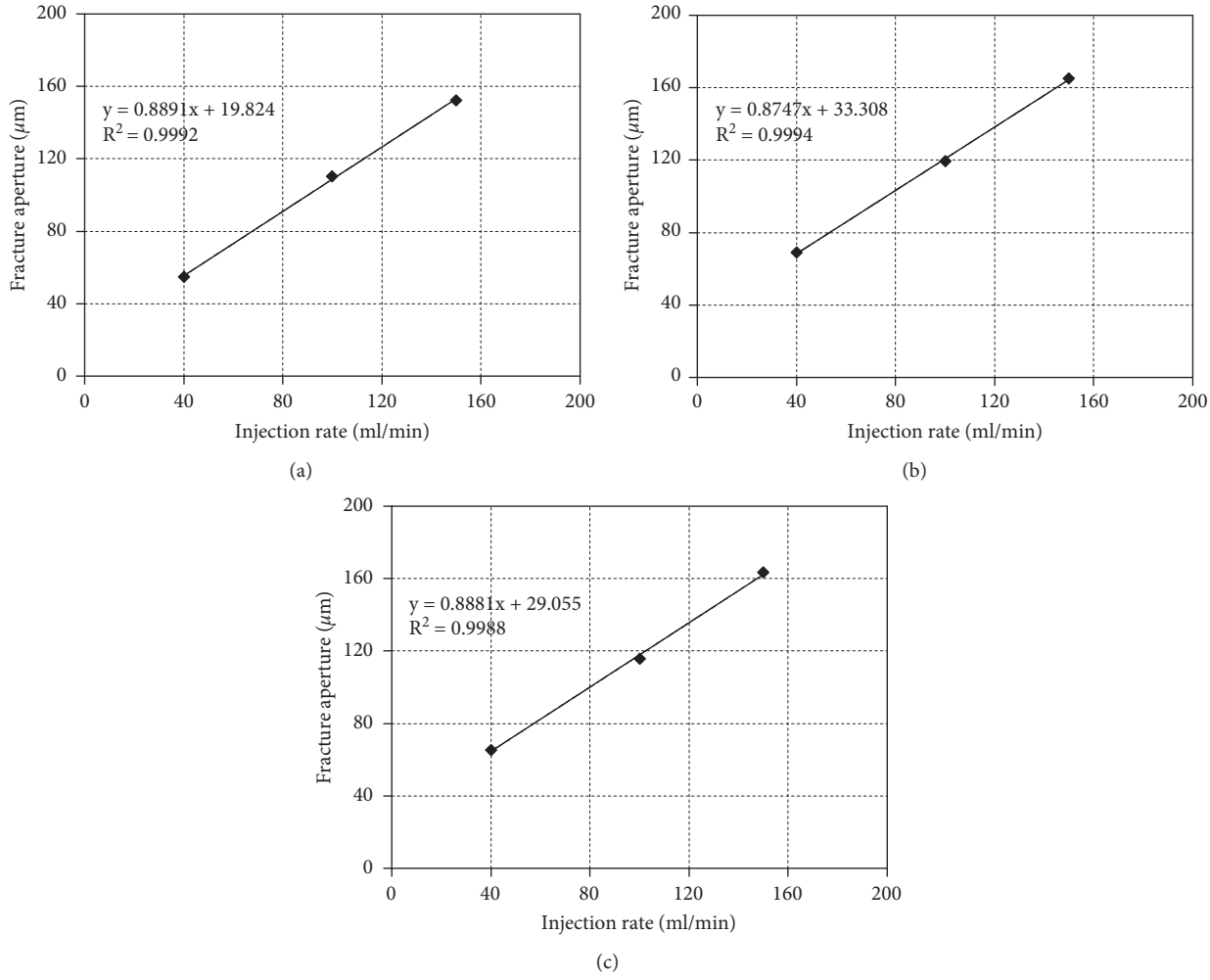

Figure 6: Relation between injection rate and fracture aperture: (a) relation between injection rate and average aperture of NOF; (b) relation between injection rate and average aperture of SNF; (c) relation between injection rate and average aperture of HF.

S3 also increase significantly, from 65.48 μm to 163.35 μm. In addition, the average value of fracture aperture of SNF is greater than that of NOF, with a ratio of 1.08 to 1.26. The reason for this could be that the SNF is generally induced by the shear mechanism, and this process is always accompanied by shear dilatancy. As shown in Figure 6, there is a significant linear relationship between injection rate and average aperture, and the linear equations are described as follows:

$$\begin{aligned} a_n &= 0.8891Q + 19.824, \\ a_s &= 0.8747Q + 33.308, \\ a &= 0.8881Q + 29.055, \end{aligned} \tag{1}$$

where a_n represents the average aperture of NOF, a_s represents the average aperture of SNF, a represents the average aperture of HF, and Q represents the injection rate.

It can be seen from Figure 7 that, for S1, the HF apertures are mainly concentrated in the three intervals of 1–50 μm, 51–100 μm, and 101–150 μm, and the sum of the frequencies is 90.8%. Especially, in the interval 1–50 μm, the frequency is 53.9%. For S2, the HF apertures are also concentrated in these three intervals, and the maximum interval of the aperture is 101–150 μm. For S3, unlike the first two specimens, the apertures are more evenly distributed in seven intervals and close to the normal distribution. In these intervals, the three intervals of 101–150 μm, 151–200 μm, and

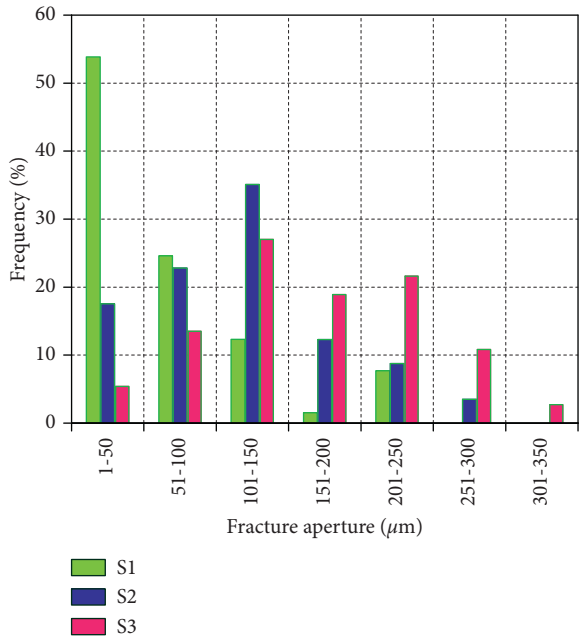

Figure 7: Distribution frequency of HF aperture.

201–250 μm are the most, with frequencies of 27%, 18.9%, and 21.6%, respectively.

4. Conclusion

Injection rate is critical for hydraulic fracturing operation because it can influence the characteristics of hydraulic fractures, such as aperture, scale, and complexity. In this study, hydraulic fracturing experiments were carried out on shale specimens to investigate the influence of injection rate on hydraulic fracture aperture. The following conclusions can be drawn:

(1) The injection rate has an obvious positive effect on hydraulic fracture aperture. When the injection rate increases, the average aperture of hydraulic fracture, both of NOF and SNF, shows a significant linear increase. The equation of average aperture and injection rate can be obtained by linear fitting.

(2) For different injection rate, the average aperture of SNF is always greater than that of NOF, with a ratio of 1.08 to 1.26. The reason could be that the SNF is generally induced by the shear dilatancy mechanism.

(3) For the largest injection rate, 150 ml/min, its corresponding fracture apertures are evenly distributed in more intervals and approximately conform to the normal distribution.

Data Availability

All the data used to support the findings of the study have been included within the article.

Conflicts of Interest

The authors declare no conflicts of interest.

Acknowledgments

This work was supported by Guizhou Science and Technology Foundation, China (Grant nos. [2019]1169 and [2019]1173), Guizhou Education Department Foundation for Youth, China (Grant no. [2018]151), Natural Science Foundation of Guizhou Minzu University (Grant no. GZMU[2019]YB27), and Scientific Research Platform of Guizhou Minzu University (GZMUSYS[2021]01).

References

[1] A. Trembath, J. Jenkins, T. Nordhaus, and M. Schellenberger, *Where the Shale Gas Revolution Came from*, Breakthrough Institute, Oakland, USA, 2012.

[2] C. Clark, A. Burnham, C. Harto, and R. Horner, *Hydraulic Fracturing and Shale Gas Production: Technology, Impacts, and Regulation*, Agronne National Laboratory, Chicago, USA, 2013.

[3] J. He, Y. Zhang, C. Yin, and X. Li, "Hydraulic fracturing behavior in shale with water and supercritical CO_2 under triaxial compression," *Geofluids*, vol. 2020, Article ID 4918087, 2020.

[4] J. E. Olson, B. Bahorich, and J. Holder, "Examining hydraulic fracture-natural fracture interaction in hydrostone block experiments," in *Proceedings of the SPE Hydraulic Fracturing Technology Conference*, vol. 152618, 2012.

[5] N. Zangeneh, E. Eberhardt, and R. M. Bustin, "Investigation of the influence of natural fractures and in situ stress on hydraulic fracture propagation using a distinct-element approach," *Canadian Geotechnical Journal*, vol. 52, no. 7, pp. 926–946, 2015.

[6] Y. Zheng, J. Liu, and Y. Lei, "The propagation behavior of hydraulic fracture in rock mass with cemented joints," *Geofluids*, vol. 2019, Article ID 5406870, 2019.

[7] H. Bao, K. K. Zhang, C. G. Yan, H. X. Lan, F. Q. Wu, and H. Zheng, "Excavation damaged zone division and time-dependency deformation prediction: A case study of excavated rock mass at Xiaowan Hydropower Station," *Engineering Geology*, vol. 272, Article ID 105668, 2020.

[8] H. Bao, Y. Zhai, H. Lan, K. Zhang, Q. Qi, and C. Yan, "Distribution characteristics and controlling factors of vertical joint spacing in sand-mud interbedded strata," *Journal of Structural Geology*, vol. 128, Article ID 103886, 2019.

[9] G. E. King, "Thirty years of gas shale fracturing: what have we learned?" in *Proceedings of the SPE Annual Technical Conference and Exhibition*, vol. 133456, SPE, Florence, Italy, 2010.

[10] X. Zhou and T. J. Burbey, "Fluid effect on hydraulic fracture propagation behavior: a comparison between water and supercritical CO2-like fluid," *Geofluids*, vol. 14, no. 2, pp. 174–188, 2014.

[11] X. Zhang, Y. Zhang, and B. Huang, "Investigation of the fracturing effect induced by the disturbing stress of hydrofracturing using the bonded-particle model," *Geofluids*, vol. 2021, Article ID 9988748, 2021.

[12] C. J. De Pater and L. J. L. Beugelsdijk, "Experiments and numerical simulation of hydraulic fracturing in naturally fractured rock," in *Proceedings of the 40th US Symposium on Rock Mechanics*, Anchorage, USAARMA 05-780, Anchorage, USA, 2005.

[13] T. Guo, S. Zhang, Z. Qu, T. Zhou, Y. Xiao, and J. Gao, "Experimental study of hydraulic fracturing for shale by

stimulated reservoir volume," *Fuel*, vol. 128, pp. 373–380, 2014.

[14] Y. Zou, S. Zhang, T. Zhou, X. Zhou, and T. Guo, "Experimental investigation into hydraulic fracture network propagation in gas shales using CT scanning technology," *Rock Mechanics and Rock Engineering*, vol. 49, no. 1, pp. 33–45, 2016.

[15] Y. Wang, X. Li, and C. A. Tang, "Effect of injection rate on hydraulic fracturing in naturally fractured shale formations-a numerical study," *Environmental Earth Sciences*, vol. 75, no. 11, pp. 1–16, 2016.

[16] J. H. Seong, S. Y. Tae, Y. K. Kwang, and G. J. Sung, "Experimental study of pumping rate effect on hydraulic fracturing of cement paste and mortar," *Rock Mechanics and Rock Engineering*, vol. 50, no. 11, pp. 3115–3119, 2017.

[17] Z. Song, Y. Wang, H. Konietzky, and X. Cai, "Mechanical behavior of marble exposed to freeze-thaw-fatigue loading," *International Journal of Rock Mechanics and Mining Sciences*, vol. 138, Article ID 104648, 2021.

[18] Y. Wang, H. N. Yang, J. Q. Han, and C. Zhu, "Effect of rock bridge length on fracture and damage modeling in granite containing hole and fissures under cyclic uniaxial increasing-amplitude decreasing-frequency (CUIADF) loads," *International Journal of Fatigue*, vol. 138, Article ID 106741, 2022.

[19] L. Bortolan Neto and A. Kotousov, "Residual opening of hydraulically stimulated fractures filled with granular particles," *Journal of Petroleum Science and Engineering*, vol. 100, pp. 24–29, 2012.

[20] C. Lin, J. He, and X. Li, "Width evolution of the hydraulic fractures in different reservoir rocks," *Rock Mechanics and Rock Engineering*, vol. 51, no. 5, pp. 1621–1627, 2018.

[21] Y. Gu, W. Ding, Q. Tian et al., "Developmental characteristics and dominant factors of natural fractures in lower Silurian marine organic-rich shale reservoirs: A case study of the Longmaxi formation in the Fenggang block, southern China," *Journal of Petroleum Science and Engineering*, vol. 192, Article ID 107277, 2020.